A New Modeling Method and Controller Design for a DC-DC Zeta Converter

Elshan Davaran Hagh[1], Ebrahim Babaei[*2], Leila Mohammadian[3]

Faculty of Electrical and Computer Engineering, University of Tabriz, Tabriz, Iran

*Corresponding Author: e-babaei@tabrizu.ac.ir

Abstract

In this paper, a new method based on signal flow graph technique and Mason's gain formula are applied to model a dc-dc Zeta converter. The model is the transfer functions from control to output and from input to output. Zeta converter is a rather complex system, which has four passive elements and may perform in either buck or boost operating modes. Compared with other converters in the same group, such as Cuk and SEPIC converters, the dynamic modelling and analysis of the Zeta converter have been not reported in the literature. For modelling target and to get rid of complex equations in modelling, a new method based on signal flow graph approach is applied to manipulate the equations. After modelling and doing dynamic stability analysis in continuous conduction mode, and prove the necessity of a controller design for it. A model based PID controller is designed for the converter and the simulation results are presented to verify the correctness of the achieved model and model- based controller and the signal flow graph performance.

Keywords

Mason Gain Formula; Model- Based Controller; Modelling; Stability Analysis; Signal Flow Graph; Zeta Converter

Introduction

Nowadays, the dc-dc converters have mostly used in many applications such as a power supply in electronic systems. In the portable devices with the battery, the converter converts the input voltage to the proper output voltage to use it by the electronic load. The battery voltage can vary in a wide range depending on a charge level. At the low charge level, it may drop below the load voltage. Thus, to continue supplying the constant load voltage, the converter must be able to work in both step-up and step-down modes. In this paper, the Zeta converter is chosen to investigate. Zeta converter is a forth order dc-dc converter which is capable of bucking or boosting the input voltage. In order to provide an inside view of the converter's action, and obtain the needed information for controller design, modelling plays an important role [1].

Modelling dc-dc converters is an effective way to get open-loop frequency response and investigate the stability of the closed-loop systems. Modelling is the first stage for designing compensator or controller circuits. Previous works present different models for dc-dc converters [2]. Considering that the power electronic converters include nonlinear elements like switches and diodes, then modelling of them needs linearization. So, applying averaging and linearization techniques has a special importance. After linearization, the inside model of the system is extractable and therefore investigating the frequency response will be possible [3-5]. Modelling dc-dc converters by using small signal linearization and averaging techniques cause complexity in the obtained equations. Solving these equations for basic converters like; buck, boost and buck-boost is not a problem, but for high order converters, dealing with them will be more difficult [6]. In [7- 8], in order to derive a mathematical model of a dc-dc converter and study the transient states of it, a combination of Laplace and Z-transforms has been employed. A converter including switches is a nonlinear system, but it can be decomposed to two linear circuits; one for on-state and the other for off-state of the switch. These two linear circuits are illustrated by means of two signal flow graphs. Composition of two sub-graphs by using switching branches reaches to the graph of the whole converter. Switching branches are the only nonlinear parts of the converters. Thus modelling process is limited to the switching branches. In [9- 12], a signal flow graph method has been presented for modelling a dc-dc converter, then by using Mason's gain formula any desired transfer function of the system might be extracted and used to design any proper controller, but the presented graph method gets a sophisticated process to achieve the small

signal model. The proposed technique in this paper, gives greatly simplified mathematical and graphical representation of the system and is based on signal flow graph of the converter. This method has great advantage because of simplicity and being capable of giving any desired transfer function of the system to design a controller for a determined variable. Graphical modelling technique is used for surveying nonlinear and dynamic behavior of switching converters. This type of converter has different configurations and all have linear subsystems [13]. The aim of this paper is to derive the model of the Zeta converter by using the proposed signal flow graph based method. The open-loop system has some disadvantages. For example, the output cannot be compensated or controlled if there is a variation or disturbance at the input. For the case of Zeta converter, the changes in the input voltage or the load current will cause the converter's output voltage to deviate from the desired value. To design a proper controller or compensator a good model of the system is needed to investigate the stability by using different tools. One of these tools is frequency domain analysis [14-15]. In order to get frequency response of the converters, after modelling the root-locus plots and the frequency domain response in form of Bode magnitude and phase diagrams are achieved and analyzed.

Many control strategies have been presented to obtain the desired output voltage in dc-dc converters. In past, the controller design was based on using small signal linearization. Linear PID and PI controllers of the converters are usually designed by using standard frequency response techniques based on small signal model of the converter by using linear control theories such as Ziegler-Nichol's method, root locus technique, hysteresis method, Bode plot and etc. The Ziegler-Nichols method is an experimental one that is widely used.

The main contribution of this paper is to derive the model of the converter using the presented signal flow graph method and then designing a model- based controller for the Zeta converter. In this process, by applying the mentioned signal flow graph technique and Mason's gain formula, the input to output, control to output transfer functions are obtained. Then, the frequency domain responses in form of Bode magnitude and phase diagrams are achieved and the proper tuned PID controller is designed. At last, the simulation results based on the presented modeling and controlling methods are brought to show the good performance and behavior of the modeling and control methods.

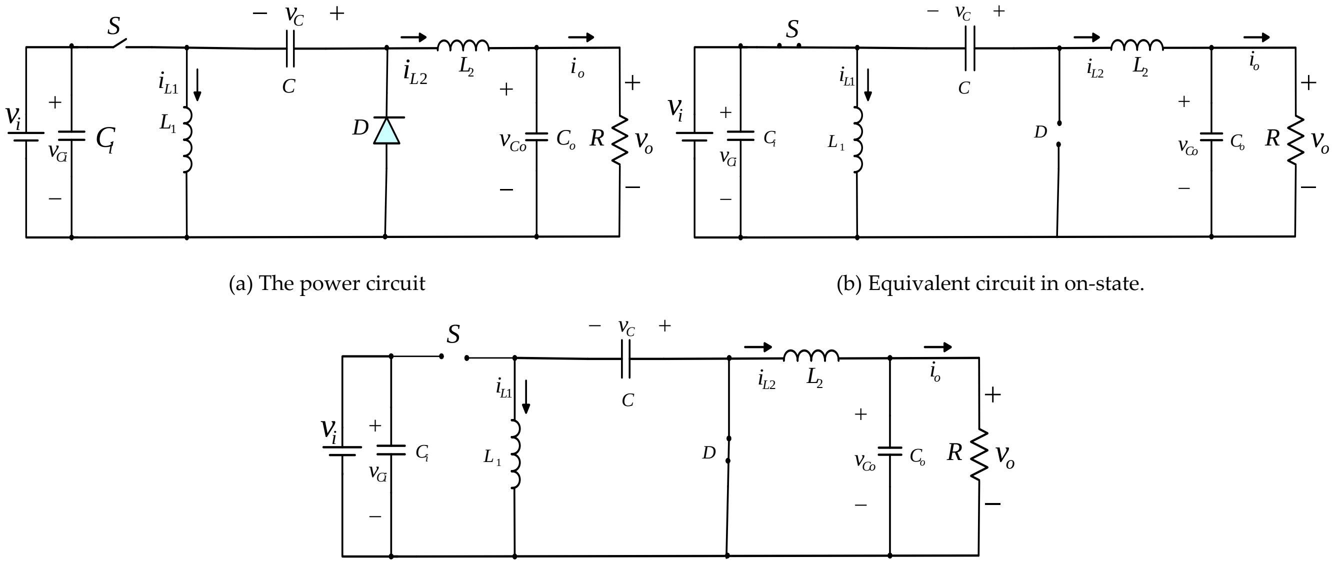

(a) The power circuit

(b) Equivalent circuit in on-state.

(c) Equivalent circuit in off-state.

FIG. 1. ZETA CONVERTER.

Review on DC-DC Zeta Converter

The power circuit of the Zeta converter shown in Fig. 1(a) has one switch, one diode, two inductors and two capacitors. In this figure, v_i and v_o are the source voltage and the output or load voltage, respectively. v_{Ci}, v_C and v_{Co} are the voltages on capacitors C_i, C and C_o, respectively. i_{L1} and i_{L2} are inductors currents. The load is

supposed as a resistor, R . Zeta converter can perform to generate a positive voltage of the input voltage which can be less or higher than input. The converter acts in two operating modes, one of them is related to on-state and the other is the off-state of the switch. Figs. 1(b) and 1(c) illustrate the equivalent circuits of the on-state and off- state operating modes, respectively.

Extraction of the State Equations

Here, the open-loop performance characteristics of the converter are tested. The starting point is the extracting a mathematical and analytical model of the system. The model is a mathematical description of the behaviour of the real system that is enough for performing stability test.

The state equations are extracted by using kirchhoff's voltage and current laws for the two cases of on and off states of the switch. These equations are calculated in loops and nodes with just one passive element, so all obtained equations are first order ones. One of the advantages of this method is in high order circuits, with increasing the order of the circuit and energy saving elements, the all extracted state equations will be of the first order and reduce the complexity of the equations and ease the analysis. The state equations are extracted for two operating modes. The first mode is when the switch is on and the diode is off, and the second mode refers to the case that the switch is in off-state and the diode conducts. The state equations for the circuit shown in Fig. 1(b) are as follows:

$$L_1 \frac{di_{L1}}{dt} = v_i \tag{1}$$

$$L_2 \frac{di_{L2}}{dt} = v_i + v_C - v_o \tag{2}$$

$$C \frac{dv_C}{dt} = -i_{L2} \tag{3}$$

$$v_o = v_{Co} \tag{4}$$

$$C_o \frac{dv_{Co}}{dt} = i_{L2} - \frac{v_o}{R} \tag{5}$$

Substituting Eq. (4) in Eq. (5), the following equation is achieved:

$$C_o \frac{dv_o}{dt} = i_{L2} - \frac{v_o}{R} \tag{6}$$

The state equations for the case that the switch is off and the diode conducts (Fig. 1(c)) are as below:

$$L_1 \frac{di_{L1}}{dt} = -v_C \tag{7}$$

$$L_2 \frac{di_{L2}}{dt} = -v_o \tag{8}$$

$$C \frac{dv_C}{dt} = i_{L1} \tag{9}$$

$$v_o = v_{Co} \tag{10}$$

$$C_o \frac{dv_{Co}}{dt} = i_{L2} - \frac{v_o}{R} \tag{11}$$

Substituting Eq. (10) in Eq. (11), the following equation is achieved:

$$C_o \frac{dv_o}{dt} = i_{L2} - \frac{v_o}{R} \tag{12}$$

Extraction of the Averaged State Equations

The state equations at the on time interval of the switch is multiplied by $\bar{d}$ and at the off time interval is multiplied by $1-\bar{d}$, then they are added to each other. $\bar{d}$ is considered as the switch conduction coefficient and $1-\bar{d}$ as the switch non-conduction coefficient. $\bar{d}$ can vary in 0 and 1 interval.

In the following equations, the variables in form of $\bar{x}$ are average values which are different from the instantaneous variables in form of x. As mentioned above, Eq. (1) to Eq. (3) and Eq. (6) are multiplied by $\bar{d}$, and Eq. (7) to Eq. (9) and Eq. (12) are multiplied by $1-\bar{d}$. Then sum of the couples will be calculated and the result is the averaged state equations. Hence, the averaged equations are related to both on and off time intervals of the switch as follows:

$$L_1\frac{d\bar{i}_{L1}}{dt} = \bar{d}\bar{v}_i - (1-\bar{d})\bar{v}_C \tag{13}$$

$$L_2\frac{d\bar{i}_{L2}}{dt} = \bar{d}\,\bar{v}_i + \bar{d}\,\bar{v}_C - \bar{v}_o \tag{14}$$

$$C_o\frac{d\bar{v}_o}{dt} = \bar{i}_{L2} - \frac{\bar{v}_o}{R} \tag{15}$$

$$C\frac{d\bar{v}_C}{dt} = -\bar{d}\,\bar{i}_{L2} + (1-\bar{d})\bar{i}_{L1} \tag{16}$$

Small Signal Linearization

In averaged state equations, dc and ac variables are substituted and rewritten with $\bar{X}$ and $\tilde{x}$, respectively. Considering all variables in form of $x = \bar{X} + \tilde{x}$, Eq. (13) to Eq. (16) are rewritten as below:

$$L_1 s(\tilde{i}_{L1} + \bar{I}_{L1}) = (\bar{D} + \tilde{d})(\tilde{v}_i + \bar{V}_i) - (1 - \bar{D} - \tilde{d})(\tilde{v}_C + \bar{V}_C) \tag{17}$$

$$L_2 s(\tilde{i}_{L2} + \bar{I}_{L2}) = (\bar{D} + \tilde{d})(\tilde{v}_i + \bar{V}_i) + (\bar{D} + \tilde{d})(\tilde{v}_C + \bar{V}_C) - \tilde{v}_o - \bar{V}_o \tag{18}$$

$$C_o s(\tilde{v}_o + \bar{V}_o) = \tilde{i}_{L2} + \bar{I}_{L2} - \frac{\tilde{v}_o}{R} - \frac{\bar{V}_o}{R} \tag{19}$$

$$Cs(\tilde{v}_C + \bar{V}_C) = -(\bar{D} + \tilde{d})(\tilde{i}_{L2} + \bar{I}_{L2}) + (1 - \bar{D} - \tilde{d})(\tilde{i}_{L1} + \bar{I}_{L1}) \tag{20}$$

The product of two dc variables is a dc one and the product of one dc and one ac variable is an ac variable, also the product of two ac variables is zero. Thus, Eq. (17) to Eq. (20) are obtained as below:

$$L_1 s\tilde{i}_{L1} = \bar{D}\tilde{v}_i + (\bar{V}_i + \bar{V}_C)\tilde{d} - (1-\bar{D})\tilde{v}_C \tag{21}$$

$$L_2 s\tilde{i}_{L2} = \bar{D}\tilde{v}_i + (\bar{V}_i + \bar{V}_C)\tilde{d} + \bar{D}\tilde{v}_C - \tilde{v}_o \tag{22}$$

$$C_o s\tilde{v}_o = \tilde{i}_{L2} - \frac{\tilde{v}_o}{R} \tag{23}$$

$$Cs\tilde{v}_C = -\bar{D}\tilde{i}_{L2} - (\bar{I}_{L2} + \bar{I}_{L1})\tilde{d} + (1-\bar{D})\tilde{i}_{L1} \tag{24}$$

Using dc equations, $\bar{V}_C$, $\bar{I}_{L1}$ and $\bar{I}_{L2}$ values versus $\bar{V}_i$ and $\bar{D}$ are calculated as follows:

$$\bar{V}_C = \frac{\bar{D}\bar{V}_i}{1-\bar{D}} \tag{25}$$

$$\overline{V}_o = \overline{D}\overline{V}_i + \overline{D}\overline{V}_C = \frac{\overline{D}\overline{V}_i}{1-\overline{D}} \tag{26}$$

$$\overline{I}_{L2} = \frac{\overline{V}_o}{R} = \frac{\overline{D}\overline{V}_i}{R(1-\overline{D})} \tag{27}$$

$$\overline{D}\overline{I}_{L2} = (1-\overline{D})\overline{I}_{L1} \tag{28}$$

$$\overline{I}_{L1} = \frac{\overline{D}}{1-\overline{D}}\overline{I}_{L2} = \frac{\overline{V}_i\overline{D}^2}{R(1-\overline{D})^2} \tag{29}$$

Considering $\overline{V}_C$, $\overline{I}_{L1}$ and $\overline{I}_{L2}$ values and replacing them in Eq. (21) to Eq. (24) and simplifying them, the small signal ac equations are calculated as below:

$$s\tilde{i}_{L1} = \frac{\overline{D}}{L_1}\tilde{v}_i + \frac{\overline{V}_i}{L_1(1-\overline{D})}\tilde{d} - \frac{1-\overline{D}}{L_1}\tilde{v}_C \tag{30}$$

$$s\tilde{i}_{L2} = \frac{\overline{D}}{L_2}\tilde{v}_i + \frac{\overline{V}_i}{L_2(1-\overline{D})}\tilde{d} + \frac{\overline{D}}{L_2}\tilde{v}_C - \frac{1}{L_2}\tilde{v}_o \tag{31}$$

$$s\tilde{v}_o = \frac{1}{C_o}\tilde{i}_{L2} - \frac{1}{RC_o}\tilde{v}_o \tag{32}$$

$$s\tilde{v}_C = -\frac{\overline{D}}{C}\tilde{i}_{L2} - \frac{\overline{V}_i}{RC(1-\overline{D})^2}\tilde{d} + \frac{1-\overline{D}}{C}\tilde{i}_{L1} \tag{33}$$

Proposed Signal Flow Graph

The ac small signal equations given in Eq. (30) to Eq. (33) are used to plot the signal flow graph as shown in Fig. 2. In these equations, there are four variables; $\tilde{v}_o$, $\tilde{i}_{L1}$, $\tilde{i}_{L2}$ and $\tilde{v}_C$, and two inputs; $\tilde{d}$ and $\tilde{v}_i$. The graph is depicted for all independent variables $(s\tilde{x}, \tilde{x})$ by using nodes and paths between two nodes. In order to extract the transfer functions from signal flow graph, the Mason gain formula will be used.

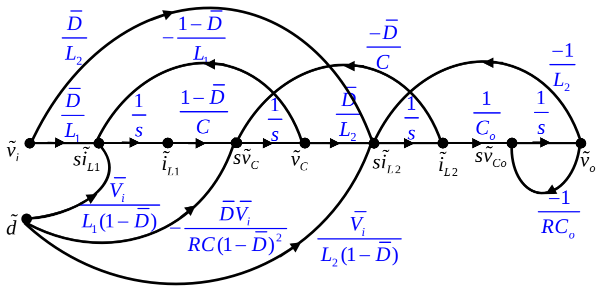

FIG. 2. SIGNAL FLOW GRAPH FOR ZETA CONVERTER.

Extracting Transfer Functions Based on the Proposed Method

For calculating the transfer functions, first the gain of distinct loops, non-touching loops and forward paths from each input to output are extracted as Table 1.

Transfer functions $\tilde{v}_o/\tilde{v}_i$ and $\tilde{v}_o/\tilde{d}$ are calculated by using Mason's gain formula $\left(y_{out}/y_{in} = \sum_{k=1}^{n} P_k\Delta_k/\Delta \right)$. In this formula, n is the number of forward paths from input to the output and Δ is calculated as follows:

$$\begin{aligned}\Delta = 1 &- \sum(\textit{distinct loops gain}) \\ &+ \sum(\textit{double nontouching loops gain}) \\ &- \sum(\textit{tripple nontouching loops gain}) + \cdots\end{aligned}$$

Omitting the path P_{i1}, $\Delta_1 = 1$ is obtained, and omitting the path P_{i2}, $\Delta_2 = 1 - Loop_1$ is obtained. Replacing the obtained values, the transfer function $\tilde{v}_o/\tilde{v}_i$ will be as shown in Table 1. Omitting the path P_{d1}, $\Delta_1 = 1$ is obtained, and omitting the path P_{d2}, $\Delta_2 = 1$ is obtained. Also, removing P_{d3}, $\Delta_3 = 1 - Loop_1$ is achieved. Replacing the obtained values, the transfer function $\tilde{v}_o/\tilde{d}$ will be obtained as given in Table1.

TABLE 1. TRANSFER FUNCTION EXTRACTION PROCESS FROM SIGNAL FLOW GRAPH OF ZETA CONVERTER

Distinct loops	**Distinct loops gain**	**Non-touching loops gain**
$Loop_1 : s\tilde{i}_{L1}, \tilde{i}_{L1}, s\tilde{v}_C, \tilde{v}_C, s\tilde{i}_{L1}$ $Loop_2 : s\tilde{v}_C, \tilde{v}_C, s\tilde{i}_{L2}, \tilde{i}_{L2}, s\tilde{v}_C$ $Loop_3 : s\tilde{i}_{L2}, \tilde{i}_{L2}, s\tilde{v}_o, \tilde{v}_o, s\tilde{i}_{L2}$ $Loop_4 : s\tilde{v}_o, \tilde{v}_o, s\tilde{v}_o$	$Loop_1 = -\frac{(1-\overline{D})^2}{L_1Cs^2}$ $Loop_2 = -\frac{\overline{D}^2}{L_2Cs^2}$ $Loop_3 = -\frac{1}{L_2C_os^2}$ $Loop_4 = -\frac{1}{RC_os}$	$Loop_{1,3} = \frac{(1-\overline{D})^2}{L_1L_2CC_os^4}$ $Loop_{1,4} = \frac{(1-\overline{D})^2}{RL_1CC_os^3}$ $Loop_{2,4} = \frac{\overline{D}^2}{RL_2CC_os^3}$

Forward paths

Paths from $\tilde{v}_i$ to $\tilde{v}_o$	**Gain**
$P_{i1} : \tilde{v}_i, s\tilde{i}_{L1}, \tilde{i}_{L1}, s\tilde{v}_C, \tilde{v}_C, s\tilde{i}_{L2}, \tilde{i}_{L2}, s\tilde{v}_o, \tilde{v}_o$ $P_{i2} : \tilde{v}_i, s\tilde{i}_{L2}, \tilde{i}_{L2}, s\tilde{v}_o, \tilde{v}_o$	$P_{i1} = \frac{\overline{D}^2(1-\overline{D})}{L_1L_2CC_os^4}$ $P_{i2} = \frac{\overline{D}}{L_2C_os^2}$

Forward paths

Paths from $\tilde{d}$ to $\tilde{v}_o$	**Gain**
$P_{d1} : \tilde{d}, s\tilde{i}_{L1}, \tilde{i}_{L1}, s\tilde{v}_C, \tilde{v}_C, s\tilde{i}_{L2}, \tilde{i}_{L2}, s\tilde{v}_o, \tilde{v}_o$ $P_{d2} : \tilde{d}, s\tilde{v}_C, \tilde{v}_C, s\tilde{i}_{L2}, \tilde{i}_{L2}, s\tilde{v}_o, \tilde{v}_o$ $P_{d3} : \tilde{d}, s\tilde{i}_{L2}, \tilde{i}_{L2}, s\tilde{v}_o, \tilde{v}_o$	$P_{d1} = \frac{\overline{V}_i\overline{D}}{L_1L_2CC_os^4}$ $P_{d2} = -\frac{\overline{V}_i\overline{D}^2}{(1-\overline{D})^2RL_2CC_os^3}$ $P_{d3} = \frac{\overline{V}_i}{(1-\overline{D})L_2C_os^2}$

Transfer function from $\tilde{v}_i$ to $\tilde{v}_o$

$$\frac{\tilde{v}_o}{\tilde{v}_i} = \sum\frac{P_i\Delta_i}{\Delta}$$

$$= \frac{P_{i1} + P_{i2}(1 - Loop_1)}{1 - Loop_1 - Loop_2 - Loop_3 - Loop_4 + Loop_{1,3} + Loop_{1,4} + Loop_{2,4}}$$

$$= \frac{\left(\frac{\overline{D}}{L_2C_o}\right)s^2 + \left(\frac{\overline{D}(1-\overline{D})}{L_1L_2CC_o}\right)}{s^4 + \left(\frac{1}{RC_o}\right)s^3 + \left(\frac{(1-\overline{D})^2}{L_1C} + \frac{\overline{D}^2}{L_2C} + \frac{1}{L_2C_o}\right)s^2 + \left(\frac{(1-\overline{D})^2}{RL_1CC_o} + \frac{\overline{D}^2}{RL_2CC_o}\right)s + \left(\frac{(1-\overline{D})^2}{L_1L_2CC_o}\right)}$$

Transfer function from $\tilde{d}$ to $\tilde{v}_o$

$$\frac{\tilde{v}_o}{\tilde{d}} = \sum\frac{P_d\Delta_d}{\Delta}$$

$$= \frac{P_{d1} + P_{d2} + P_{d3}(1 - Loop_1)}{1 - Loop_1 - Loop_2 - Loop_3 - Loop_4 + Loop_{1,3} + Loop_{1,4} + Loop_{2,4}}$$

$$= \frac{\left(\frac{\overline{V}_i}{(1-\overline{D})L_2C_o}\right)s^2 - \left(\frac{\overline{V}_i\overline{D}^2}{(1-\overline{D})^2RL_2CC_o}\right)s + \left(\frac{\overline{V}_i}{L_1L_2CC_o}\right)}{s^4 + \left(\frac{1}{RC_o}\right)s^3 + \left(\frac{(1-\overline{D})^2}{L_1C} + \frac{\overline{D}^2}{L_2C} + \frac{1}{L_2C_o}\right)s^2 + \left(\frac{(1-\overline{D})^2}{RL_1CC_o} + \frac{\overline{D}^2}{RL_2CC_o}\right)s + \left(\frac{(1-\overline{D})^2}{L_1L_2CC_o}\right)}$$

TABLE 2. SIMULATION PARAMETERS

L_1	L_2	C	C_1
$18.9\,\mu H$	$18.9\,\mu H$	$14\,\mu F$	$11.2\,\mu F$
C_o	R_o	v_i	d
$6.5\,\mu F$	10Ω	$12V$	0.57

TABLE 3. INFORMATION OBTAINED FROM POLES AND ZEROS OF THE TRANSFER FUNCTION OF $\tilde{v}_o/\tilde{v}_i$

	Poles		Zeros
Value	-1.15×10^3 $\pm2.45\times10^4 i$	-6.54×10^3 $\pm9.69\times10^4 i$	$\pm4.03\times10^4 i$
Damping	0.047	0.0673	0
Overshoot (%)	86.3	80.9	100
Frequency (rad/s)	2.46×10^4	9.71×10^4	4.03×10^4

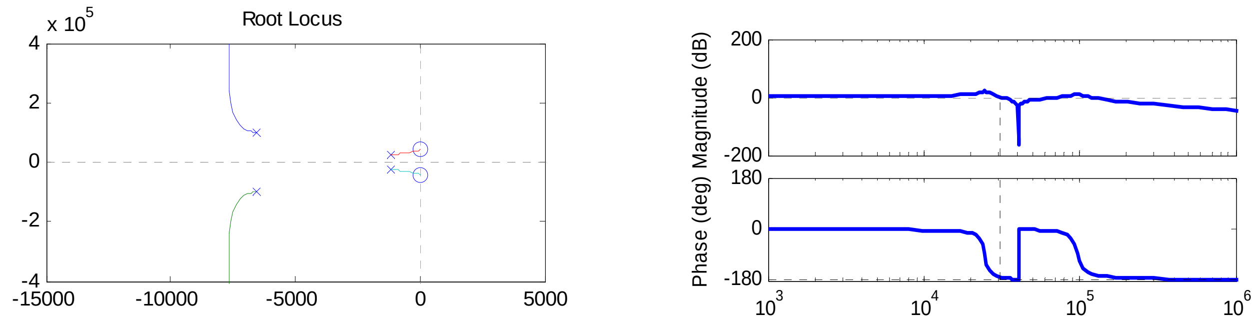

(a) ROOT LOCUS (b) BODE DIAGRAMS

FIG 3. RESPONSE OF TRANSFER FUNCTION OF $\tilde{v}_o/\tilde{v}_i$

Simulation Results

In simulation, the parameters of Zeta converter are considered as given in Table 2.

Frequency Response Analysis for $\tilde{v}_o/\tilde{v}_i$ Transfer Function

The root-locus, magnitude and phase Bode diagrams for extracted transfer function of $\tilde{v}_o/\tilde{v}_i$ are shown in Fig. 3. The information obtained from these diagrams is given in Table 3.

Considering the root-locus shown in Fig. 3(a), it is understood that $\tilde{v}_o/\tilde{v}_i$ has four complex poles in left hand side of the imaginary axis and two complex zeros on imaginary axis. Considering Bode diagrams (Fig. 3(b)), the magnitude curve of the function begins with a constant value of $2.64dB(DC\,gain)$ and at the frequency of $24.6\,kHz$ duo to the poles $-1.15\times10^3\pm2.45\times10^4 i$, an undershoot occurs in magnitude curve and its slope becomes $-40\,dB/dec$ and the phase curve begins from 0^o and a phase reduction of -180^o takes place. At the frequency of $40.3kHz$ duo to the zeros $\pm4.03\times10^4 i$ on imaginary axis, an overshoot occurs in magnitude curve and $+40\,dB/dec$ is added to its slope. So, the slope becomes zero and $+180^o$ is added to phase curve duo to the mentioned zeros. Finally at frequency $97.1\,kHz$ because of the poles $-6.54\times10^3\pm9.69\times10^4 i$, an undershoot occurs in magnitude curve and its slope becomes $-40\,dB/dec$ and at the phase curve a phase reduction of -180^o takes place and the phase becomes -180^o.

Considering the plotted responses for all values of the gain, the transfer function $\tilde{v}_o/\tilde{v}_i$ is stable and gain margin becomes ∞. Considering Bode diagram, when the magnitude is $0\,dB$, the phase equals to 171^o, so the phase margin which equals to the difference of 180^o and this phase will be 9^o.

2) Frequency Response Analysis for $\tilde{v}_o/\tilde{d}$ Transfer Function

The root-locus and Bode diagrams for the extracted transfer function of $\tilde{v}_o/\tilde{d}$ are shown in Fig.4. The information obtained from these diagrams is given in Table 4.

Considering the root-locus shown in Fig. 4(a), it is understood that $\tilde{v}_o/\tilde{d}$ has four complex poles in left hand side

of the imaginary axis and two complex zeros right hand plane. From Bode diagrams (Fig. 4(b)), gain margin of the system is $-37.5\,dB$ and the phase margin is 2.52^{o}. So, the transfer function is unstable and needs a compensator in normal conditions.

From root-locus diagrams, the mentioned system has two complex zeros in right hand side of the imaginary axis. In order to have a more stable system the proper controller should be designed for the mentioned transfer function. In next section designing the proposed model- based PID controller will be explained.

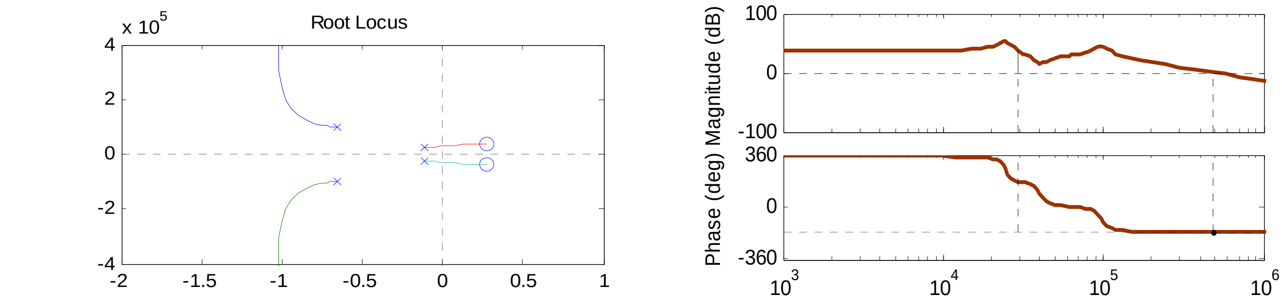

(a) ROOT LOCUS (b) BODE DIAGRAMS

FIG 4. RESPONSE OF TRANSFER FUNCTION OF $\tilde{v}_o/\tilde{d}$

TABLE 4. INFORMATION OBTAINED FORM POLES AND ZEROS OF THE TRANSFER FUNCTION OF $\tilde{v}_o/\tilde{d}$

	Poles		Zeros
Value	-1.15×10^{3} $\pm2.45\times10^{4}i$	-6.54×10^{3} $\pm9.69\times10^{4}i$	2.7×10^{3} $\pm4.03\times10^{4}i$
Damping	0.047	0.0673	−0.0669
Overshoot (%)	86.3	80.9	123
Frequency (rad/s)	2.46×10^{4}	9.71×10^{4}	4.03×10^{4}

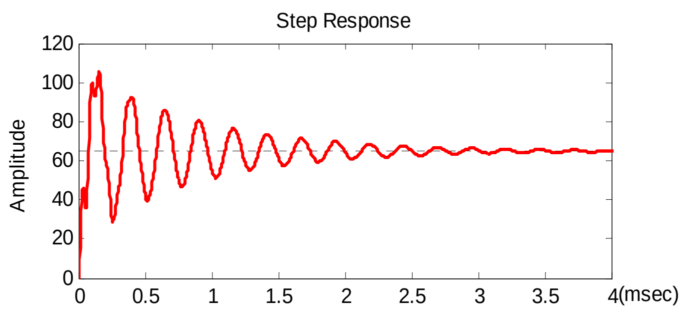

FIG. 5. STEP RESPONSE OF THE OPEN LOOP SYSTEM

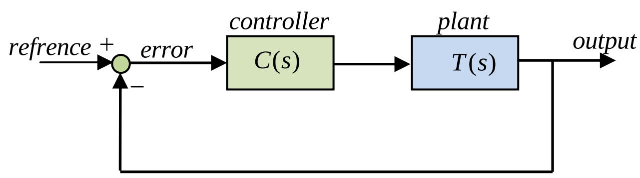

FIG. 6. THE WHOLE SYSTEM CONFIGURATION WITH THE PID CONTROLLER

The Proposed Model-Based Controller

Fig. 5 shows the step response of the system. This shows that the open-loop system does not reject disturbances on the input voltage and cannot regulate the output voltage.

At the following, a model-based PID controller by using Ziegler-Nichol's tuning method will be explained.

The whole configuration of the controller beside the controlled system is plotted in Fig. 6. In order to control the converter based on the previously extracted model, the PID controller is added to the controlled transfer function of the converter.

The PID controllers are widely used because they have only three parameters that has to be tuned for the process control. The input of a PID controller is an error signal which is the difference between the measured value and a desired reference signal for a process variable. The controller minimizes the error by tuning three constant parameters namely the proportional term (K_P), the integral term (K_I) and the differential term (K_D). Because of its simple configuration, the PID controller is the most commonly used control method in industry. The important

aims of the PID controllers are:

- eliminating steady-state error of the step response (due to the integral action)
- reducing the peak overshoot (providing damping due to derivative action)

There are many methods for tuning the PID parameters or gains. The most famous method for achieving the mentioned goal is Ziegler-Nichols tuning method. Table 6 shows the parameters obtained for the controller.

Fig. 7 shows the step response of the system after applying the designed PID controller.

Fig. 8 shows the Bode diagrams of the system before and after applying the designed PID controller. Fig. 9 shows the Nyquist diagram of the closed loop system. The results prove the stability of the obtained system with the proposed controller. Stability of the obtained controlled system is well illustraited in Fig. 9.

From the simulation results, it is obvious that the disturbance is rejected and this controller behaves very desirably in time-domain. Checking the bode diagrams depicts that the system has become a stable one. Also, calculations bring out the gain margin as $16.2dB$ and a phase margin of $89.7\deg$ which are favorite frequency-domain response characteristics. Then, applying the proposed controller, the converter system becomes stable and regulated.

TABLE 6. PID PARAMETERS OBTAINED

K_P	0
K_I	8.0306
K_D	0
Rise time of closed loop response	0.00422
Settling time of closed loop response	0.00748
Overshoot of closed loop response	0
Gain Margin of closed loop response	16.2
Phase Margin of closed loop response	89.7
Closed loop stable?	Yes

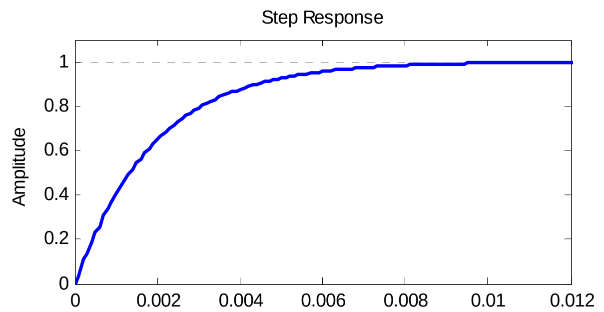

FIG. 7. STEP RESPONSE OF THE CLOSED LOOP CONVERTER SYSTEM

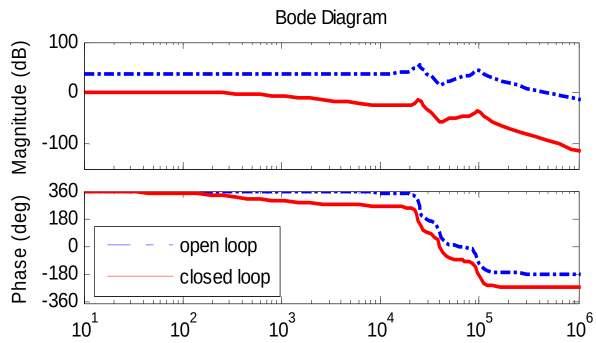

FIG. 8. BODE DIAGRAMS OF THE OPEN LOOP AND CLOSED LOOP CONVERTER SYSTEM

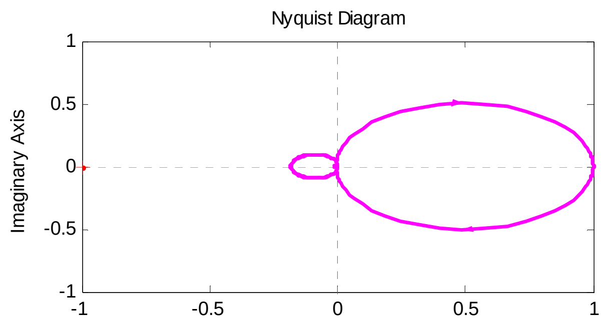

FIG. 9. NYQUIST DIAGRAM OF THE CLOSED LOOP CONVERTER SYSTEM

Conclusions

In this paper, modelling and analyzing of the Zeta converter operating in continuous conduction mode were presented. Application of the proposed based on signal flow graph method and Mason's gain formula for extracting associated transfer functions and modelling a dc-dc Zeta converter was investigated. In this process, for modelling the average and small signal linearization techniques were employed. Extracting the final transfer functions from initial state space equations were described step by step. Application of signal flow graph method and Mason's rule helps to solve the high order complex equations simply. The presented method deals with the equations with more state variables as well. In this paper, the transfer functions from input to output and control to output were obtained. Then, by using the proposed method the poles, zeros, root-locus plot and Bode diagrams were extracted and the achieved frequency response was analyzed. Finally, the efficiency of the proposed tuned

PID controller as a model based technique to design a proper control system is shown. The proposed control system employs the PID controller with a special adjustment for proper setting of the control responses.

REFERENCES

[1] Kapat, S. Control methods for improving the performance of dc-dc converters. Ph.D. Thesis, Kharagpur, India, 2009.

[2] Gatto, G.; Marongiu, I.; Mocci, A.; Serpi, A. "An improved averaged model for boost dc-dc converters" in Proc. IECON, 412– 417, Vienna, 2013.

[3] Babaei, E.; Mashinchi Mahery, H. "Investigation of buck-boost dc-dc converter operation in DCM and the effect of converter elements on output response using mathematical model based on Laplace and Z transforms." Electric Power Components and Systems Journal, in press..

[4] Priewasser, R. Modelling, control and digital implementation of dc-dc converters under variable switching frequency operation. PhD. Thesis, Klagenfurt University, 2012.

[5] Priewasser, R.; Agostinelli, M.; Unterrieder, Ch.; Marsili, S.; Huemer, M. "Modelling, Control, and Implementation of dc–dc Converters for Variable Frequency Operation." IEEE Trans. Power Electron. vol. 29, no. 1, 287–301, 2014.

[6] Wong, L.K.; Man, T.K. "Small signal modelling of open loop SEPIC converters." IET Power Electron. vol. 3, no. 6, 858-868, 2010.

[7] Babaei, E.; Mashinchi Maheri, H. "Analytical solution for steady and transient states of buck dc–dc converter in CCM." Arab. Journal Sci. Eng., vol. 38, no. 12, 3383-3397, 2013.

[8] Mashinchi Mahery, H.; Babaei, E. "Mathematical modelling of buck–boost dc–dc converter and investigation of converter elements on transient and steady state responses." Electrical Power and Energy Systems, vol. 44, 949-963, 2013.

[9] Ki, W.H. "Signal flow graph in loop gain analysis of dc-dc PWM CCM switching converter." IEEE Trans. Circuit Sys., vol. 45, no. 6, 644-655, 1998.

[10] Smedley, K.; Cuk, S. "Switching flow graph nonlinear modelling technique." IEEE Trans. Power Electron. vol. 9, no. 4, 405-413, 1994.

[11] Veerachary, M. "General rules for signal flow graph modelling and analysis of dc-dc converters." IEEE Trans. Aerospace Electron. Sys., vol. 40, no. 1, 259–271, 2004.

[12] Veerachary, M. "Analysis of Fourth-Order DC-DC Converters: A Flow Graph Approach." IEEE Trans. Ind. Electron. vol 55, no. 1, 133-141, 2008.

[13] Palomo, R. L.; Saldan, J.A.M.; Ramos, J. L. "Signal Flow Graphs for Modelling of Switching Converters with Reduced Redundant Power Processing." IET Power Electron. vol. 5, no. 7, 1008–1016, 2012.

[14] Veerachary, M.; Singamaneni, B.S. "Stability Analysis of Cascaded DC–DC Power Electronic System." IEEJ Trans. Elec. Electron. Eng. vol. 4, no. 6, 763–770, 2009.

[15] Renaudineau, H.; Martin, J.; Mobarakeh, B.N; Pierfederici, S. "DC-DC Converters Dynamic Modelling with State Observer-Based Parameter Estimation." IEEE Trans. Power Electron. vol. 99, no. 1, 1-9, 2014.